

COMPUTATIONAL AND EXPERIMENTAL ANALYSIS OF GAS-PARTICLE FLOW IN FURNANCE POWER BOILER INSTALATIONS WITH RESPECT TO EROSION PHENOMENA

BOLESŁAW DOBROWOLSKI
JACEK WYDRYCH

Opole University of Technology, Faculty of Mechanical Engineering, Poland
e-mail: j.wydrych@po.opole.pl

The paper presents a method for finding such instalation elements which are especially subjected to erosion wear and a method for quantitative assessment of the erosion loss at a given operational time of a pneumatic conveying system. Motion of the gas is described by the Reynolds equation with the turbulence model. Motion of solid particles is described by the Lagrange equation. Then, the erosive loss of the wall material is calculated according to the Bitter model. The calculations are performed for a part of the dust system in BP-1150 boiler. It is found that a "cord" of particles is formed as a result of some changes of the flow direction inside the stream. High local intensity of particle collisions with the walls is the main reason for accelerated erosion of some parts of the system. The numerical calculation results are compared with the results of measurements on material losses of the elbow.

Key words: pneumatic transport, pulverized coal, erosion

1. Introduction

While operating furnace systems of solid-fuel power boilers, intense wear of pulverized coal system elements constitutes one of the most important problems (Dobrowolski and Wydrych, 2005, 2006). Erosive action of particles is caused by increased concentration of solid particles in some areas (Crowe, 2006; Founti *et al.*, 2001).

In the papers on erosive wear of elements of pneumatic conveying systems one can find equations determining of ann wear element versus parameters characterizing flow of the conveyed mixture and properties of frictional pairs (erodent-wall).

There are many papers concerning the flow of air-solid particles mixtures in dust pipe systems (Aroussi *et al.*, 2002; Borsuk *et al.*, 1963; Djebedjian, 2001), cyclons (Su, 2006), riser reactors (Zheng *et al.*, 2001), flows in the space between pipes (Wydrych and Szmolke, 2006) and behind spheres (Eiamworawutthikul and Gould, 2001). Their authors tested, among others, the influence of system configuration and parameters characterizing the flow on erosive wear of elements. In pneumatic conveying systems with the gas-particle flow, one may often observe inhomogeneity of particle concentration (Pachler *et al.*, 2001; Piątkiewicz, 1999) and pulverized coal pipe erosion being out of control and causing accelerated wear.

This paper presents numerical and experimental investigations on erosive wear in a part of a boiler furnace system in Opole Power Plant. Strong diversification of concentration and segregation of particles within the elbow caused inhomogeneous concentration in the mixture flow to the four-path separator located directly above the elbow. It was the reason for diversified silt of pulverized coal to the boiler corners and accelerated erosion of separators and elbows.

2. The aim of the paper and experimental methods

In order to obtain experimental data concerning erosive wear of pulverized coal systems, some measurements were done in Opole Power Plant. The measurements were a part of works performed in order to explain reasons for the non-uniformity in particles distribution in the boiler installation BP-1150. The tested installation is shown in Fig. 1. The detailed measurements were performed in the mill installation 3MW4, where a dispersing obstacle had been located before the separator in order to improve the flow conditions. Figure 2 shows geometry of the flow system and position of the dispersing element 175 mm in height (i.e. angle $\phi = 90^\circ$, and angle β is 13.5°). The flow system has the following dimensions: $D = 1200$ mm, $R = 1180$ mm, $l_w = 2000$ mm. It is the outlet straight section of the pulverized coal pipe from the mill together with the elbow. Directly under the elbow, there is a four-path separator. In the measuring sections before and behind the elbow, distributions of medium speeds and concentration were measured as well as fractional analyses of particles were performed. Numerical tests and measurements were carried out for the average loading of the mill RP1043x, i.e. 40 t/h and the air flow 70000 Nm³/h.

In order to determine the flow conditions before the elbow, measurements of the distribution of velocity and concentration of particles before the elbow were done (Dobrowolski *et al.*, 2004). The measurements were done under working conditions. The mixture flow velocity in pipes was measured with the

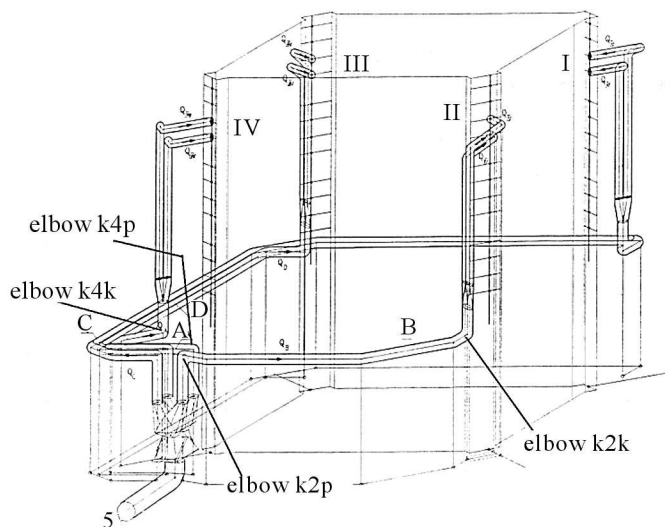


Fig. 1. Pulverized coal installation and selected elbows

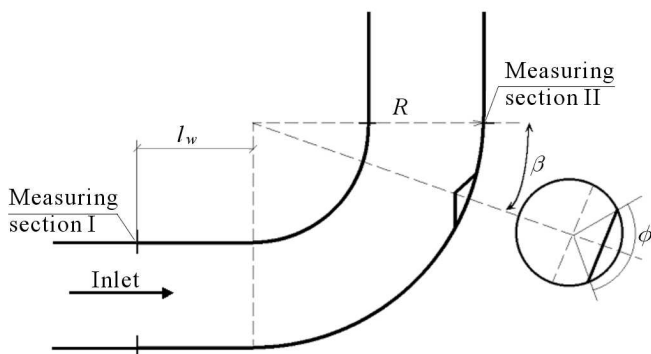


Fig. 2. Geometry of the flow system with the particle dispersing element

use of a cylindrical impact tube. The particle samples in the section before the distributor and in the inlet section were sampled with a device for isokinetic suction. The distributions of velocity and concentration of particles are shown in Fig. 3.

Similar measurements were done in the pipeline cross section just behind the elbow. The results of measurements were compared with the results of numerical calculations (see the further part of the paper).

Taking into account calculations of the erosive loss, it is necessary to know the operating conditions of the mill. For this purpose, the reports describing the working conditions of mill 4 in block 3 in Opolé Power Plant were analysed. Then, the mean values of basic operational parameters of the installation were calculated.

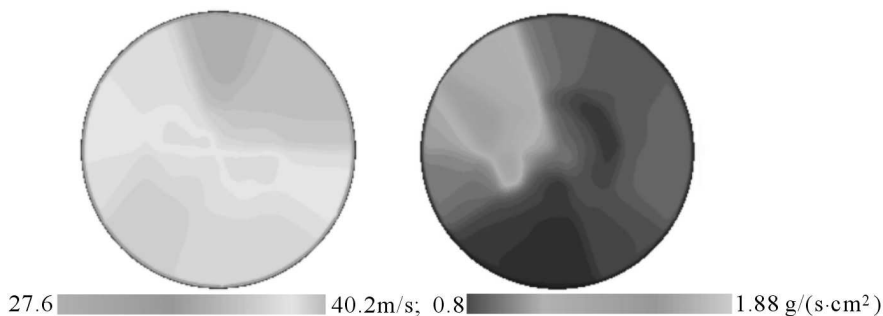


Fig. 3. Distributions of velocity and concentration of particles in the measuring section before the elbow

In this paper, the measurements were mainly realised in order to determine the erosion on the dissipative element and elbow surfaces under known flow conditions.

For determination of the erosive loss in the dispersive element, a supersonic thickness gauge with accuracy 0.01 mm was applied. While wear testing, the material of the dissipative element (steel St3S of the initial thickness 6 mm) was measured several times. The thickness was measured in 120 points forming a uniform grid on the plate surface.

While handling the mathematical data, erosive losses in mm were recalculated for volume units, and then for masses of the removed material for the measured element surface. Finally wear in g/m^2 was obtained. Analysis of the erosive losses obtained from measurements and calculations is presented in this paper.

In order to estimate the material loss on the internal surface of the elbow, a suitable measuring device was made. During the measurements, the distances between the measuring axis and the element internal walls were measured in thirty sections perpendicular to the pipeline axis.

The data from measurements were used for calculations of differences between dimensions of the elements removed from the installation and dimensions of new elements.

3. Mathematical model of flow of the air-pulverized coal mixture

In numerical calculations, a suitable mathematical model was used. The model included equations of motion for the gaseous phase and particles of pulverized coal. Air motion was described with the Euler method and particle motion – with the Lagrange method.

3.1. Equations of gas motion

Since it is possible to analyse motion of the polydispersion mixture gas-particles, in this work the PSICell method was used (Wydrych, 2002). Phase changes were neglected and it was assumed that both phases were incompressible. The flow was isothermal and steady. The steady state time-averaged conservation equations of mass and momentum can be written as

$$\begin{aligned} \frac{\partial}{\partial x_j}(\rho \bar{U}_j) &= 0 \\ \frac{\partial}{\partial x_i}(\rho \bar{U}_i \bar{U}_j) &= -\frac{\partial p}{\partial x_i} + \frac{\partial}{\partial x_j} \left(\mu \frac{\partial U_i}{\partial x_j} \right) - \frac{\partial}{\partial x_j}(\rho \overline{u_i u_j}) + \overline{S_{u_i,p}} \end{aligned} \quad (3.1)$$

where p is the static pressure and the stress tensor $\rho \overline{u_i u_j}$ is given by

$$-\rho \overline{u_i u_j} = \left[\mu_{ef} \left(\frac{\partial \bar{U}_i}{\partial x_j} + \frac{\partial \bar{U}_j}{\partial x_i} \right) \right] - \frac{2}{3} \rho k \delta_{ij} \quad (3.2)$$

where δ_{ij} is the Kronecker delta and $\mu_{ef} = \mu + \mu_t$ is the effective viscosity. The turbulent viscosity, μ_t , is calculated using the high-Reynolds number form as

$$\mu_t = C_\mu \rho \frac{k^2}{\varepsilon} \quad (3.3)$$

with $C_\mu = 0.09$, k and ε are the kinetic energy of turbulence and its dissipation rate, respectively. These were obtained by solving their conservation equations as given below. In the PSICell method it is assumed that the disintegrated phase particles are sources of mass, momentum and energy occurring as additional components of $\overline{S_{u_i,p}}$ in equations of the continuous gas phase (Crowe, 2006). The term $\overline{S_{u_i,p}}$ term is given by (Wydrych, 2002)

$$\overline{S_{u_i,p}} = \frac{1}{V_E} \eta_j \int_{\delta t_j} \frac{\mu C_D \text{Re}_p D_p}{8\pi} (\bar{u}_i - u_{pi}) dt \quad (3.4)$$

The transport equations of the turbulence model are given as follows

$$\begin{aligned} \frac{\partial}{\partial x_j}(\rho \bar{U}_j k) &= \frac{\partial}{\partial x_j} \left(\frac{\mu_{ef}}{\sigma_k} \frac{\partial k}{\partial x_i} \right) + G_k - \rho \varepsilon \\ \frac{\partial}{\partial x_j}(\rho \bar{U}_j \varepsilon) &= \frac{\partial}{\partial x_i} \left(\frac{\mu_{ef}}{\sigma_\varepsilon} \frac{\partial \varepsilon}{\partial x_i} \right) + C_1 G_k \frac{\varepsilon}{k} - C_2 \rho \frac{\varepsilon^2}{k} \end{aligned} \quad (3.5)$$

where G_k represents the generation of turbulent kinetic energy due to mean velocity gradients, and is given by

$$G_k = -\rho \overline{u_i u_j} \frac{\partial \bar{U}_j}{\partial x_i} \quad (3.6)$$

The quantities σ_k and σ_ε are the effective Prandtl numbers for k and ε . The turbulence model constants have values: $C_1 = 1.44$, $C_2 = 1.92$, $\sigma_k = 1.0$ and $\sigma_\varepsilon = 1.3$ (Wydrych, 2002).

3.2. Equation of motion and calculation of particle trajectories

In order to calculate the mentioned source components, we must know trajectories of the particle. The particle path is calculated from the equation of motion.

In some papers concerning flows of dust-gas mixtures through systems of different geometries, the forces coming from rotational motion of a solid particle are taken into account (Founti *et al.*, 2001; Heintz and Bohnet, 2005; Marchioli *et al.*, 2007; Wang and Levy, 2006). They are Saffman and Magnus forces. These forces are of a great importance in some zones, especially in layers near walls of the flow systems. In order to determine conditions for which the forces can be neglected, parametric calculations were done for the plane flow. During calculations, a gas-particles flow connected with a direction change was considered. A scheme of the system was shown in Fig. 4.

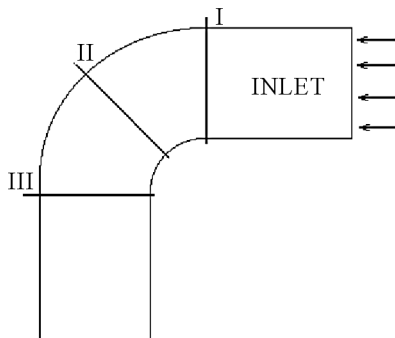


Fig. 4. A scheme of the two-dimensional flow system

The considered system includes a pipeline interval with the diameter $D = 0.5$ m, containing an elbow with the radius of curvature 0.5 m. The inlet part length was 1 m, and the outlet part length was 1.25 m. It was assumed that at the system inlet the velocity changed within 3 - 30 m/s. Sand of break-up varying in the range of 10 - $500 \mu\text{m}$ was the solid fraction. Gas motion was described by Eq. (3.1)₂ and it was solved with use of the finite difference method and a code elaborated by the authors. Solid particle motion in the gas velocity field was described by the following equation (Wydrych, 2002)

$$m_p \frac{d\bar{u}_p}{dt} = \bar{F}_d + \bar{F}_g + \bar{F}_{ls} + \bar{F}_{lr} \quad (3.7)$$

Trajectories of particle motion were obtained as a result of integration of Eq. (3.7). The calculations were performed in order to determine forces of

aerodynamic drag \overline{F}_d , gravity \overline{F}_g , Saffman \overline{F}_{ls} and Magnus \overline{F}_{lr} in control sections I, II and III, Fig. 4 (Wydrych, 2002).

When a particle passed through the control section, values of particular forces acting on the particle were registered and used for further analysis. The obtained results of calculations were presented in form of relative forces influencing the particle. The relative aerodynamic drag was calculated from

$$F_d^w = \text{relative aerodynamic drag} = \frac{F_d}{\sum F} \tag{3.8}$$

where $\sum F$ is the sum of all forces. Relative values of other forces were calculated in a similar way. The next results of calculations corresponded to the case when the inlet was located 60 mm from the upper wall of the flow system.

From the above results, it appears that the aerodynamic drag strongly influences the particle trajectory (see Fig. 5). For particles of about 60 μm in diameter and gas velocities about 25 m/s, its participation reaches even 95%. The gravity force is the most important for big particles, bigger than 200 μm in diameter. The influence of the aerodynamic Magnus force and the Saffman force is small in the whole range of diameters and velocities of particles and can be neglected (it does not exceed 1%).

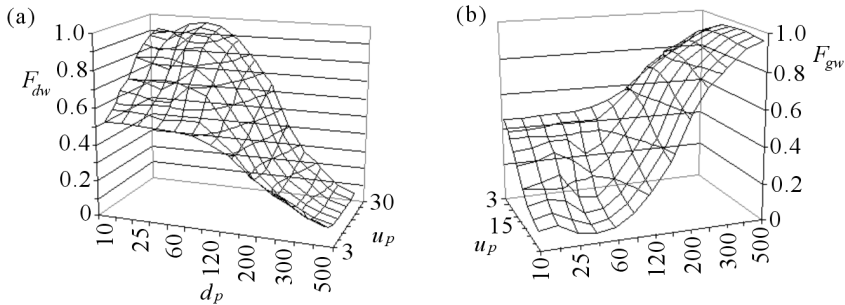


Fig. 5. Relative forces acting on the particle in control section II versus diameter and velocity of the particle; (a) aerodynamic drag, (b) gravity force

If the difference of phase densities is great, the equation of particle motion can be written as

$$m_p \frac{du_p}{dt} = \frac{3}{4} C_D \frac{\rho m_p}{\rho_p d_p} |u - u_p| (u - u_p) + g \tag{3.9}$$

where m_p is the particle mass, and C_D is the coefficient of aerodynamic drag. The above equation can be written as

$$\frac{du_p}{dt} = \frac{1}{\tau_P} (u - u_p) + g \tag{3.10}$$

when dynamic relaxation time is determined as

$$\tau_P = \frac{\rho_p d_P^2}{18\mu f} \quad (3.11)$$

Assuming that the gas velocity is constant on the elementary surface, the equation of particle motion can be solved in an analytic way, so calculations of the trajectory become easier.

3.3. Simulation of turbulent diffusion of particles

Turbulent fluctuations of the transported phase can be neglected when the time of dynamic relaxation is high in comparison with the time characterizing turbulent fluctuations (Gore and Crowe, 1989). In order to balance the effects of slip between the fluctuation of velocity and the dispersed phase, we can apply the SSF model (random separation of the flow). In such a case, it is necessary to know the main properties characterizing the turbulent flow, which can be determined at any point of the fluid from the calculated velocity field according to the extended interpolation procedure including kinetic energy k and its rate of dissipation ε .

The influence of fluctuation of the gas phase velocity on particle trajectories is included in the assumption that fluctuations of velocity are constant while the particle moves through a turbulent flow. The particle velocity is calculated including fluctuations of the gas phase velocity. The gas phase velocity can be written as a sum of the mean velocity and the fluctuation velocity $u(t) = \bar{u} + u'(t)$. Stochastic nature of the turbulence process can be modelled with so-called random walk mechanisms, including mechanisms of Discrete Random Walks (DRW) (Banderier and Krattenthaler, 2003) and Continuous Random Walks (CRW) (Bocksell and Loth, 2001).

The characteristic velocity fluctuations and the turbulence time are obtained by random selection from the probability density function for velocity. In DRW, for simplification, the velocity fluctuations are assumed as isotropic from the Gaussian probability density function with the standard deviation equal to $\sqrt{(2/3)k}$. It is assumed that the particle passes through turbulence while turbulence duration or during the time necessary for the particle to omit the turbulence. The time of cooperation between the particle and simulated turbulences is dependent on the random time of existence of the turbulences. If the random variable is less than $\Delta t/T_L$, where Δt is the time and T_L is the time scale of turbulence, a new turbulence is generated. The time scale of turbulence is calculated from kinetic energy of turbulence k and kinetic energy of turbulence ε (Volkov, 2004) according to

$$T_L = C_T \frac{k}{\varepsilon} \quad (3.12)$$

or from the following relationship

$$t_{EDDY} = \frac{L_\epsilon}{u'} = \frac{L_\epsilon}{\sqrt{\frac{2}{3}k}} \quad (3.13)$$

where C_T is experimentally estimated as 0.3 and the time scale of turbulence L_ϵ is calculated from (Volkov, 2004)

$$L_\epsilon = \frac{C_\mu^{\frac{3}{4}} k^{\frac{3}{2}}}{\varepsilon} \quad (3.14)$$

In the case of CRW, the gas phase velocity is obtained by solving the Langevin equation

$$du_i = \frac{1}{T_L} u_i dt + \sqrt{\frac{2u'_i u'_i}{T_L}} dw$$

where w is the Gaussian probability density function. Since the considered procedure is random, we must simulate motion of many particles from a single inlet, if we want to obtain representative values.

The differences in the phase densities are big, and the particles of large diameters are not very open to gas phase fluctuations (Curtis, 2003; Hardalupas and Horender, 2003; Wang *et al.*, 2006). Thus, the influence of turbulent diffusion on particle motion is neglected in the considered problem.

3.4. Modelling of collisions of particles with walls

The case when a particle collides with the solid wall should be treated with special attention. In such a case, components of the particle velocity vector after a collision are calculated from the following equations

$$u_{p1} = e_t u_p \quad v_{p1} = -e_n v_p \quad (3.15)$$

where e_t and e_n determine the coefficient of restitution in shear and normal directions to the wall surface, u_p , v_p are advanced velocities in x and y directions. In Eq. (3.15), the subscript 1 means the component of particle velocity after collision (see Fig. 6).

The coefficient of restitution e is strongly dependent on the coefficient of kinetic friction, particle velocity, glancing angle and properties of materials used for the particle and the wall. From the tests (Sommerfeld, 1992) it results that the coefficient of restitution is strongly dependent on the wall surface smoothness and the particle shape.

Relations between the coefficient of restitution and the particle glancing angle for the given material pairs were obtained during experiments. The

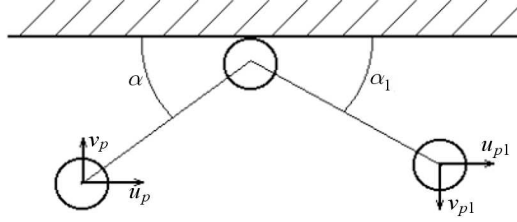


Fig. 6. Configuration of particle-wall collision with velocity notation

relations for stainless steel 410 and high-silica sand are expressed by the following equations (Sommerfeld, 1992)

$$e_t = 0.988 - 1.66\alpha + 2.11\alpha^2 - 0.67\alpha^3 \quad (3.16)$$

$$e_n = 0.993 - 1.76\alpha + 1.56\alpha^2 - 0.49\alpha^3$$

4. Models of erosive wear

Many methods of erosion velocity calculations have been proposed so far (Banderier and Krattenthaler, 2003; Deng *et al.*, 2004; ElTobgy *et al.*, 2005; Founti *et al.*, 2001; Junichi *et al.*, 2003; Kilarski *et al.*, 1998; Mazumder *et al.*, 2005, Mbabazi and Sheer, 2006). After parametric analysis of some chosen models, the authors selected Bitter's model for further considerations (Dobrowolski and Wydrych, 2005, 2006; Wydrych and Szmolke, 2006). Bitter's erosion model is a function of the particle glancing angle and function of the particle velocity.

In Bitter's model (Bitter, 1963), the erosion mechanism is classified in two categories, i.e. hearing and deformation. In both cases, the erosion process can be quantitatively described as

$$M_c = \frac{\rho_t C m_p u_p^2}{P \psi} \left[\sin 2\alpha - \frac{2}{w_y} \left(1 + \frac{m_p r_p^2}{I_p} \right) \sin^2 \alpha \right]$$

$$\text{for } \tan \alpha < \left[\frac{2}{w_y} \left(1 + \frac{m_p r_p^2}{I_p} \right) \right]^{-1}$$

$$P = \sqrt[5]{\frac{40}{\pi^4} \rho_p \left(\frac{1 - q_p^2}{E_p} + \frac{1 - q_t^2}{E_t} \right)^{-4} (u_p \sin \alpha)^2} \quad (4.1)$$

$$M_d = \frac{1}{2\varepsilon_0} \rho_p m_p (u_p \sin \alpha - u_0)^2$$

$$u_0 = \frac{\pi^2}{2\sqrt{10}} \sqrt{(1.59Y)^5 \frac{1}{\rho_p} \left(\frac{1 - q_p^2}{E_p} + \frac{1 - q_t^2}{E_t} \right)^2}$$

where:

- M_c – mass of the removed material of the wall caused by shearing erosion and calculated for a single particle collision [kg];
- M_d – mass of the removed material of the wall caused by strain erosion and calculated for a single particle collision [kg];
- r_p – radius of the particle [m];
- ρ_t – wall material density [kg/m³];
- Y – plastic stress of the wall material [J/m²];
- ψ – constant for shearing wear ($\psi = 2$);
- P – normal stress [N/m²].

Generally speaking, the shearing and strain occur together and they are probably often independent, so the total amount of the removed wall material can be written as the sum of those two fractions, $M_{er} = M_c + M_d$ (Crowe, 2006).

In the above equations, there are three experimental constants: C , w_y and ε , including all factors influencing the erosion process, i.e. the granular structure of materials of the wall and particle as well as the shape of particles. These quantities must be determined from experiments for a considered combination of materials of the particle and the wall. The following values were assumed for these constants: $C = 0.015$, $w_y = 6.0$ and $\varepsilon_0 = 7 \cdot 10^{11}$ J/m³.

5. Results of measurements and calculations of gas velocity and particle concentration

Numerical calculations for the elbow before the four-path separator were performed on a mesh containing 57268 elementary cells in total volume, while 235 cells were located on the dissipative element surface. In order to define the boundary conditions at the system outlet in the correct way, a straight interval 2000 mm long was defined behind the elbow.

For numerical calculations, suitable boundary conditions were applied. Exemplary distributions of particle velocity and concentrations obtained from measurements are shown in Fig. 3. It is possible to find high inhomogeneities of gas velocity fields and particle concentrations at the outlet of the mill. 1560 point inlets were located at the initial section for determination of particle trajectories and erosive wear. Elementary streams of particles at the inlet sections were calculated on the basis of results of measurements of particles concentration with an interpolation method.

Using the methods described in Section 3, the authors carried out a series of numerical calculations for geometry with and without dissipative element.

As a consequence, the velocity fields of the gaseous phase were obtained for the tested area (Fig. 7 and Fig. 8). Calculations were done with the FLUENT program (Fluent Inc., 2006).



Fig. 7. Gas velocity distributions in selected sections of the calculation area without the dissipative element

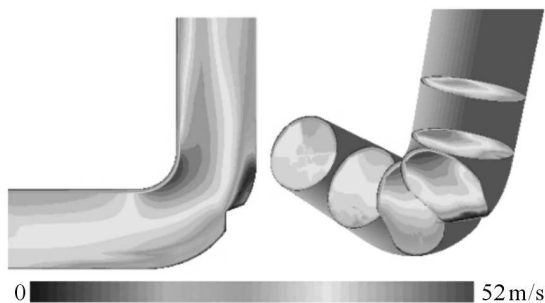


Fig. 8. Gas velocity distributions in selected sections of the calculation area with the dissipative element

From analysis of the velocity distributions shown in Fig. 7 and Fig. 8, it appears that the maximum velocity area occurs at the side of the internal elbow arc, but the zone of the decreased velocity is directly behind the dissipative element.

Strong influence of the elbow on the velocity distribution in its plane and just behind it can be seen. Velocity distributions in the pipe cross section behind the elbow, obtained from numerical calculations, are shown in Fig. 9. The same data found from the measurements are presented in Fig. 10.

From Figs. 7-10, it appears that the dissipative element strongly influences the velocity distribution behind the elbow.

After reaching convergence of the solution for the velocity fields and taking into account presence of solid particles, trajectories of particles were calculated.

The particle trajectories were used for calculations of particles concentration in selected sections. The results are presented in Fig. 11 and Fig. 12.

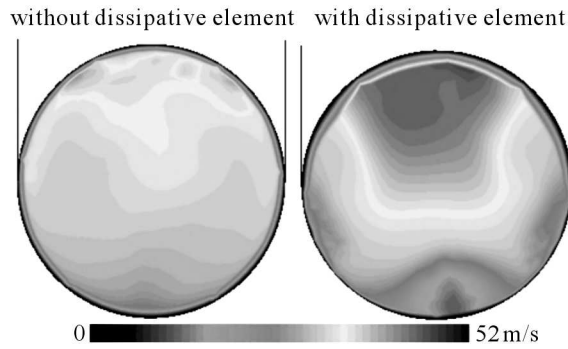


Fig. 9. Gas velocity distributions in the section behind the elbow obtained from numerical calculations

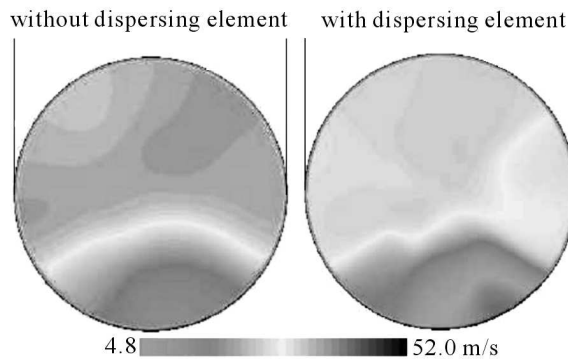


Fig. 10. Gas velocity distributions in the section behind the elbow obtained from experiments



Fig. 11. Concentration distribution for the solid fraction in selected sections of the calculation area without the dispersing element

The numerical results shown in Fig. 12 allow one to draw a conclusion that the zone of high concentration occurs in front of the dispersive element at the side of the external elbow arc.

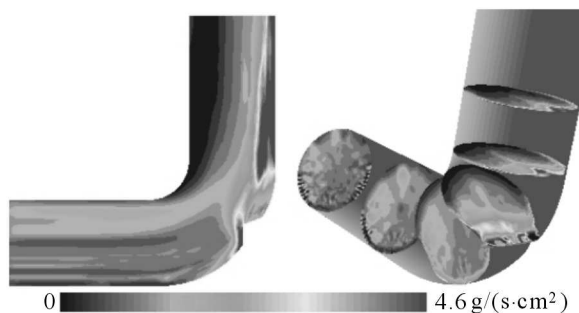


Fig. 12. Concentration distribution for the solid fraction in selected sections of the calculation area with the dispersing element

Influence of the dispersive element on the calculated distributions of concentration of the solid fraction in the section behind the elbow may be deduced from Fig. 13. Figure 14 shows the results of measurements of particle concentration in the section behind the elbow.

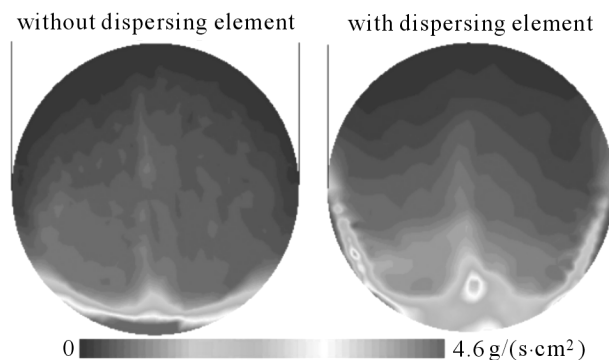


Fig. 13. Concentration distributions in the section behind the elbow obtained from numerical calculations

The results of numerical calculations shown in Figs. 11-14 allow one to assess the effect of the dispersive element on the distribution of particles concentration. Insertion of the dispersive element introduces more homogeneous concentration occurring at the side of external arc of the elbow. Qualitative similarity of the calculated and experimental results can be seen. The observed quantitative differences can result from the assumed simplifications and from possible changes of the mill load during measurements. The differences can also result from the three-dimensional nature of the flow in the considered system, so a range of applicability of the methods can be limited to measurements of velocity and concentration of the particles.

The test results obtained for fragments of the pulverized coal installation shown in Fig. 1 are presented below. Detailed calculations were performed for

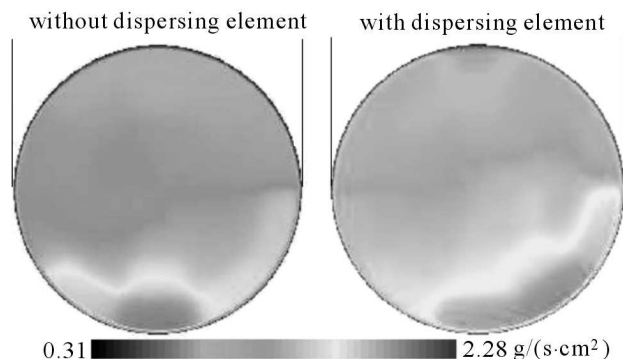


Fig. 14. Concentration distributions in the section behind the elbow obtained from experiments

part IV of the installation. There, at the inlet, the velocity distribution found numerically for the four-path distributor was given. The calculation results for velocity fields in some chosen sections of the flow system are shown in Fig. 15 and Fig. 16.

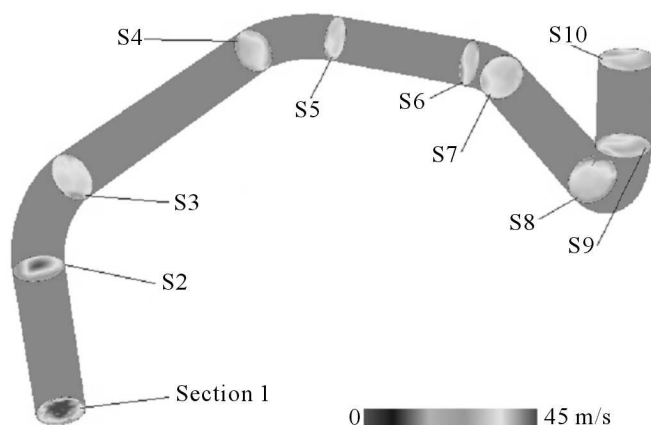


Fig. 15. Geometry of fragment IV in the pulverized coal system and control sections

Analysis of the velocity distributions in the considered system gives information about the location of zones of high and low velocities. A velocity increase can be observed at the internal sides of the elbows, and it is dependent on the change of the stream direction. Non-homogeneity of the velocity field along the whole pipeline length can be observed.

Trajectories of particles delivered to the system from 1560 inlets in section 1 were calculated in the gas velocity field. Figure 17 shows trajectories of the particles delivered to the system from inlets arranged on the pipe diameter in section S1. The particles of large diameters often move along the paths forming "a line", which causes a local increase in concentration. Figure 18

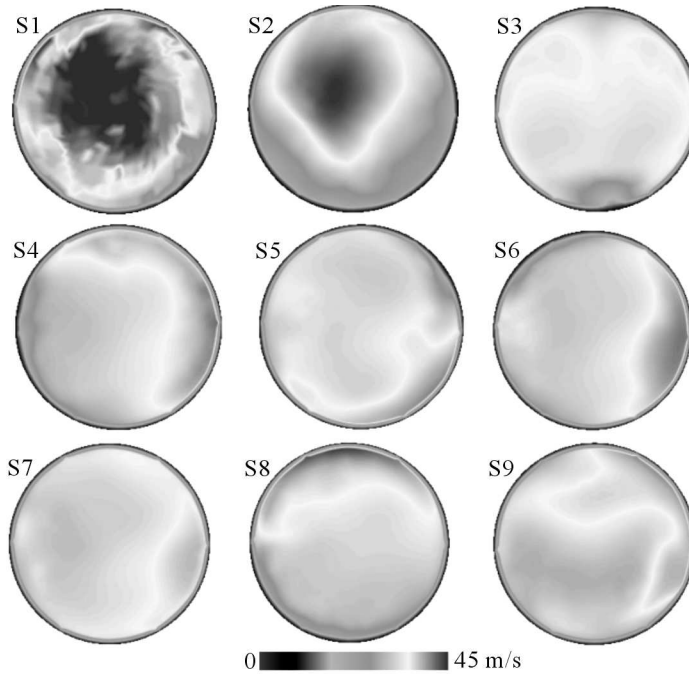


Fig. 16. Velocity distributions in chosen sections of the flow system (part IV)

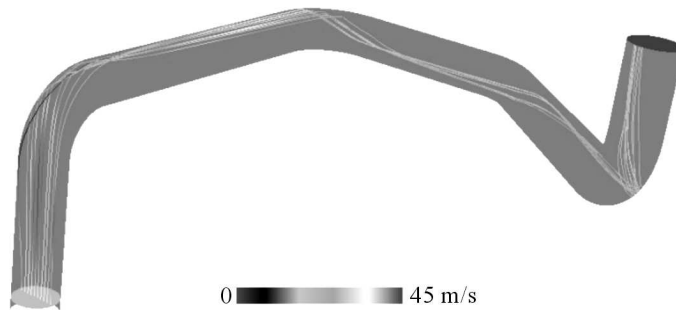


Fig. 17. Trajectories of particles $80\ \mu\text{m}$ in diameter

shows the distribution of particle concentration in some chosen sections of the flow system.

From particle concentration distributions, it appears that a change of the flow direction influences formation of high non-uniformities in straight-line intervals behind the elbows. In consequence of action of the centrifugal force, thick fractions of particles are rejected on the external surfaces, and their further movement has form of "a line". It is an unfavourable phenomenon because of particle segregation, it also causes excessive wear of the surfaces of the installation elements in some areas. The previously presented model of

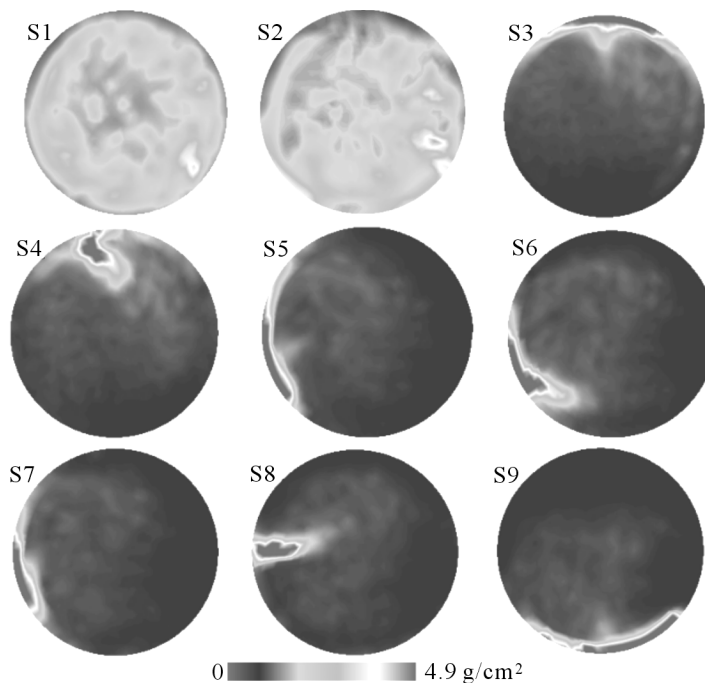


Fig. 18. Distribution of the solid phase concentration in some chosen sections of the flow system (part IV)

erosion was used for calculations of erosion losses on the walls of the pulverized coal system.

6. Results of measurements and calculations on erosive wear

This Section presents results of measurements and calculations on erosion wear of the tested parts of the pulverized coal installation. Figure 19 shows distribution of erosion wear in part IV of the pulverized coal system.

Thus, it is possible to find zones of the maximum erosion wear on the surface of part IV, i.e. on the external surfaces of the elbow arcs. On the elbow k4_45_2, the zone of the maximum wear is displaced toward the lower external part of the elbow. It is caused by lowering the "line" of particles due to the gravity force. Erosion wear can also be seen in some areas of straight sections between the elbows. Wear at those sections is caused by erosion action of large particles rejected from the external elbow arcs. A pronounced wear zone can be observed just before the elbow 4k, which is a result of rejection of particles from the elbow k4_45_2.

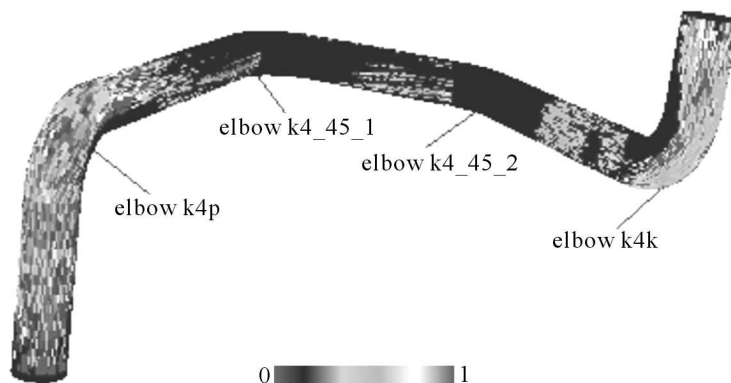


Fig. 19. Normalized distribution of erosion wear of the internal surface in part IV of the pulverized coal system

In the further part of the paper, one can find results of measurements and calculations on erosion wear in one chosen elbow of the tested pipeline. It is the elbow with the internal angle of 90° , located in part IV of the boiler pulverized coal installation.

From numerical calculations (Fig. 20) it appears that the maximum wear occurs on side surfaces of the external arc of the elbow, just behind the elbow. Figure 20 shows a zone of increased erosion wear in the initial elbow part, being a result of action of the four-path separator, located just before the inlet section.

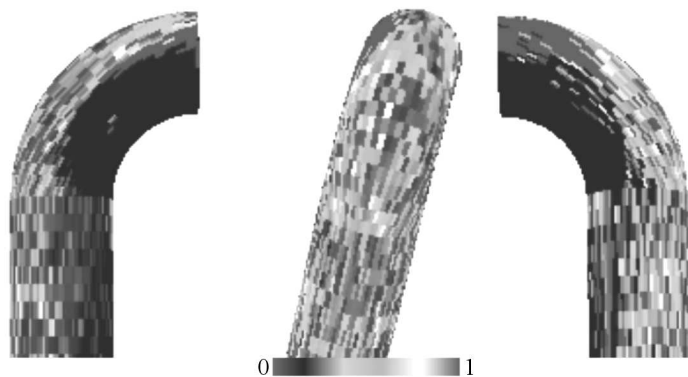


Fig. 20. Normalized distribution of erosion wear on the elbow surface k4p obtained from numerical calculations

The experiments prove increased wear of the external elbow arc and occurrence of increased erosion in the inlet part of the elbow. At both sides of the elbow, in its inlet part there are zones of maximum wear in form of strips (see Fig. 21). It is caused by the fact that the elbow k4p is located just behind

the four-path separator which causes non-uniform distributions of velocity and concentration of the solid phase in the inlet section of part IV.

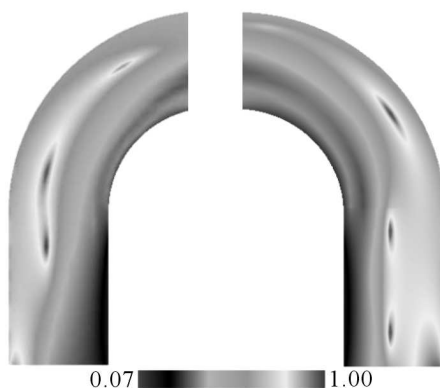


Fig. 21. Normalized distribution of erosion wear on the elbow surface k4p obtained from experiments

The location of the dissipative element (Fig. 2) causes its increased wear on the wall subjected to the particles action. The intensity of wear of the wall allows one to determine dynamics of development of the zones with increased erosive wear.

Basing on theoretical considerations presented in previous Sections, the authors carried out numerical calculations on erosive wear of the dissipative element.

In order to calculate the erosive wear rate for the dispersing element we assumed that pulverized coal contains 7% quartz. Further calculations were realized only for particles of quartz as the main factor causing erosive wear. The calculations were done for 13 different diameters of the particles: $2.5\ \mu\text{m}$, $5\ \mu\text{m}$, $10\ \mu\text{m}$, $15\ \mu\text{m}$, $25\ \mu\text{m}$, $40\ \mu\text{m}$, $60\ \mu\text{m}$, $90\ \mu\text{m}$, $120\ \mu\text{m}$, $150\ \mu\text{m}$, $200\ \mu\text{m}$, $300\ \mu\text{m}$, and $400\ \mu\text{m}$ assuming fraction distributions resulting from the experiments. These data were used for determination of mass and percentage fractions of particular fractions of pulverized coal in the point of measurements with the Rosin-Rammler-Sperling method. The remainder on the screen $0.2\ \text{mm}$ was 2%, and on the screen $0.09\ \text{mm}$ – 20%. The erosive wear rate was calculated with the FLUENT program (Fluent Inc., 2006), completed with our own UDF procedure extending capability of the original code.

For each fraction, the wear rate of the dissipative element was calculated. Next, we calculated the total element wear being a sum of erosive action of particular fractions. The data for all the fractions, including periods of different operational conditions were applied to calculations of the total rate of erosive wear per unit surface (Fig. 22).



Fig. 22. Total velocity of erosive wear of the wall material used in the dissipative element for the Bitter model of wear

Figure 23 presents the erosive wear distribution for the dissipative element obtained during measurements with the ultrasonic thickness gauge with accuracy 0.01 mm in g/m^2 for two times of element operation, 3963 and 7320 h.

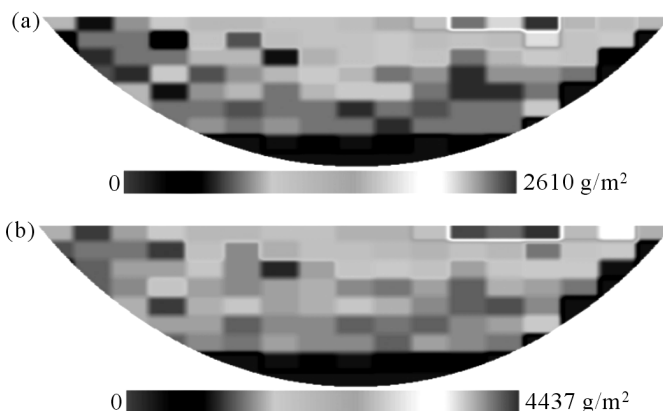


Fig. 23. Distribution of erosive wear of the wall material of the dissipative element obtained from experiments for two operating times: (a) 3936 h and (b) 7320 h

The measurement results prove strong asymmetry of the wear zone distribution resulting from non-uniformity of the distributions of velocity and concentration of the solid phase behind the coal mill. The results obtained from numerical calculations show increased wear in the whole element area, but the experimental results do not prove it.

Figure 23 gives information about dynamics and changes in the location of wear zones on the dispersive element surface. One can observe that the maximum wear zone is located on the right side of the central part of the plate and it does not displace itself while operating. It means that for the considered system the conditions at the inlet are restored to the previous ones.

7. Conclusions

The effects of flow velocity and concentration of particles on erosion in the boiler furnace system were investigated for a special case of flow with a low particle concentration. The calculations were done for a system including a dissipative element and for fragments of a pulverized coal installation with elbows. Concentrations of particle velocity and concentrations in the investigated fragments were calculated.

The results of numerical calculations allow one to assess the influence of the dispersive element on the distribution of particles concentration. Insertion of the dispersive element causes that the loss of high concentration occurring at the side of the external arc of the elbow has a greater range. Qualitative similarity of the calculated and experimental results can be seen. It was also found that asymmetry of the erosive wear distribution observed on the "threshold" surface resulted from the velocity field asymmetry and particle concentration in the inlet section.

Analysis of the velocity distributions for the installation section with elbows gave information about the location of zones of high and low velocities. A velocity increase could be observed at the internal sides of the elbows, and it was dependent on the angle of the stream direction change. Non-homogeneity of the velocity field along the whole pipeline length was observed.

From the particle concentration distributions it appears that a change of the flow direction influences formation of high non-uniformities in straight intervals behind the elbows. As a consequence of action of the centrifugal force, bigger fractions of particles are rejected on the external surfaces, and their further movement has form of "a rope". It is a unfavourable phenomenon because of particle segregation, it also causes excessive wear of surfaces of the installation elements in some areas. From numerical calculations it appears that the zone of maximum erosive wear occurs in the area of the external elbow arc. The results of experiments prove the occurrence of increased wear at the external elbow arc. The measurement also prove a displacement of the maximum wear zone toward the external elbow arc.

Further numerical calculations seem to be reasonable. They should enable optimum selection of materials and geometries ensuring longer life of the installation elements and lower diversification of the solid phase concentration in the tested areas.

Notations

- C_1, C_2, C_μ – empirical constants of turbulence model
 C_D – coefficient of aerodynamic drag

d_p	–	particle diameter
e_t, e_n	–	restitution ratios
f	–	empirical function
$\overline{F}_d, \overline{F}_g$	–	drag and gravitational force, respectively
$\overline{F}_{ls}, \overline{F}_{lr}$	–	Saffman and Magnus lift force, respectively
k	–	kinetic energy of turbulence
M_c, M_d	–	mass removed by cutting and deformation wear, respectively
m_p	–	mass of particles
p	–	pressure
P	–	normal stress
r_p	–	radius of particle
$\overline{S}_{u_i, p}$	–	additional component dependent on phase particles as sources of momentum
u, u_p	–	gas and particle velocity vector, respectively
u_i	–	gas velocity vector components in index notation
Y	–	plastic stress of wall material
δ_{ij}	–	Kronecker delta
ε	–	turbulence energy dissipation rate
μ, μ_{ef}, μ_t	–	dynamic, effective and turbulent viscosity, respectively
ρ, ρ_p	–	fluid and particle density, respectively
ρ_t	–	density of wall material
$\sigma_k, \sigma_\varepsilon$	–	turbulent Prandtl and turbulent Schmidt number, respectively
τ_p	–	dynamic relaxation time
ψ	–	cutting wear constant.

References

1. AROUSSI A., GIDDINGS D., MOZAFFARI E., PICKERING S.J., 2002, Characterisation of pulverised fuel roping, *15th International Congress of Chemical and Process Engineering (CHISA2002)*, Prague, Czech Republic
2. BANDERIER C., KRATTENTHALER CH., 2003, —em Discrete Random Walks, DRW'03, Discrete Mathematics and Theoretical Computer Science, Conference Volume AC, 259-264
3. BITTER J.G.A., 1963, A study of erosion phenomena, *Wear*, **6**, p. 5
4. BORSUK G., DOBROWOLSKI B., WYDRYCH J., 2006, Gas-solids mixture flow through a two-bend system, *Chemical and Process Engineering*, **27**, 645-656
5. BOCKSELL T.L., LOTH E., 2001, Random walk models for particle diffusion in free-shear flows, *AIAA Journal*, **39**, 6, 1086-1096

6. BRACH R.M., 1997, Impact coefficients and tangential impacts, *Transactions of the ASME – Journal of Applied Mechanics*, **64**, 4, 1014-1016
7. CROWE C.T., 2006, *Multiphase Flow Handbook*, Taylor and Francis Group
8. CURTIS J.S., 2003, Effect of solids loading, Reynolds number, and particle size distribution on velocity fluctuations in gas-particle flows, *4th ASME-JSME Joint Fluids Engineering Conference Honolulu*, Hawaii, USA
9. DENG T., BINGLEY M.S., BRADLEY M.S.A., 2004, The influence of particle rotation on the solid particle erosion rate of metals, *Wear*, **256**, 1037-1049
10. DJEBEDJIAN B., 2001, Numerical and experimental investigations of turbulent flow in a 180° curved diffuser, *ASME Division of Fluid Dynamics Summer Meeting*, New Orleans, LA
11. DOBROWOLSKI B., POSPOLITA J., WYDRYCH J., 2004, Próba poprawy warunków przepływowych przed rozdzielaczem czterodrogowym w układzie pyłowym kotła BP-1150, *Inżynieria Chemiczna i Procesowa*, **25**, 4, 2105-2112
12. DOBROWOLSKI B., WYDRYCH J., 2005, Prognozowanie zużycia erozyjnego układów transportu pneumatycznego w energetyce, *VII Konferencja "Problemy Badawcze Energetyki Ciepłej"*, Warszawa
13. DOBROWOLSKI B., WYDRYCH J., 2006, Evaluation of numerical models for prediction of areas subjected to erosion wear, —em *Int. J. of Applied Mechanics and Engineering*, **11**, 4, 735-749
14. EIAMWORAWUTTHIKUL C., GOULD R.D., 2001, Wake behind a sphere in low Reynolds number turbulent freestream, *ASME Division of Fluid Dynamics Summer Meeting*, New Orleans, LA
15. ELTOBGY M.S., NG E., ELBESTAWI M.A., 2005, Finite element modeling of erosive wear, *International Journal of Machine Tools and Manufacture*, **45**, 1337-1346
16. *Fluent Inc.*, 2006, *Fluid Dynamics Analysis Package*, Fluid Dynamic Internationale Inc.
17. FOUNTI M.A., KOLAITIS D.I., KATSOURINIS D.I., 2001, Particle induced erosion wear in a sudden expansion flow and in a long pipe transporting crude oil, *ASME Division of Fluid Dynamics Summer Meeting*, New Orleans, LA
18. GORE R.A., CROWE C.T., 1989, Effect of particle size on modulating turbulent intensity, *Int. J. Multiphase Flow*, **15**, 279-285
19. HARDALUPAS Y., HORENDER S., 2003, Fluctuations of particle concentration in a turbulent two-phase shear layer, *International Journal of Multiphase Flow*, **29**, 1645-1667
20. HEINL E., BOHNET M., 2005, Calculation of particle-wall adhesion in horizontal gas-solids flow using CFD, *Powder Technology*, **159**, 2, 95-104
21. JUNICHI K., TODA K., YAMAMOTO M., 2003, Development of numerical code to predict three-dimensional sand erosion phenomena, *4th ASME-JSME Joint Fluids Engineering Conference Honolulu*, Hawaii, USA

22. KILARSKI J., JURA S., STUDNICKI A., SUCHOŃ J., 1998, Problem trwałości separatorów palników pyłowych, *VI Forum Energetyków "Gospodarka Remontowa Energetyki"*, Politechnika Opolska, Opole, 185-188
23. MARCHIOLI C., PICCIOTTO M., SOLDATI A., 2007, Influence of gravity and lift on particle velocity statistics and transfer rates in turbulent vertical channel flow, *International Journal of Multiphase Flow*, **33**, 227-251
24. MAZUMDER Q.H., SHIRAZI S.A., MCLAURY B.S., SHADLEY J.R., RYBICKI E.F., 2005, Development and validation of a mechanistic model to predict solid particle erosion in multiphase flow, *Wear*, **259**, 203-207
25. MBABAZI J.G., SHEER T.J., 2006, Computational prediction of erosion of air heater elements by fly ash particles, *Wear*, **261**, 1322-1336
26. PACHLER K., BERNERT K., FRANK TH., SCHNEIDER H., 2001, Numerical simulation of disperse multiphase flows with an application in power engineering, *3rd Int. Symp. Comp. Tech. Fluid/Thermal/Chemical Systems Ind. Appl.*, Atlanta, Georgia, USA
27. PIĄTKIEWICZ Z., 1999, *Transport pneumatyczny*, Monografie, Wydawnictwo Politechniki Śląskiej, Gliwice
28. RANI S.L., WINKLER C.M., VANKA S.P., 2004, Numerical simulations of turbulence modulation by dense particles in a fully developed pipe flow, *Powder Technology*, **141**, 80-99
29. SOMMERFELD M., 1992, Modelling of particle-wall collisions in confined gas-particle flows, *Int. J. Multiphase Flow*, **18**, 6, 905-926
30. SU Y., 2006, The turbulent characteristics of the gas-solid suspension in a square cyclone separator, *Chemical Engineering Science*, **61**, 1395-1400
31. VOLKOV K.N., 2004, Stochastic modeling of impurity motion and scattering in the mechanics of turbulent gas-dispersed flows, *Journal of Engineering Physics and Thermophysics*, **77**, 5
32. VOLKOV K. N., 2004, Influence of turbulence on the deposition of particles from a gas-dispersed flow on the wall, *Journal of Engineering Physics and Thermophysics*, **77**, 5
33. WANG J., LEVY E.K., 2006, Particle behavior in the turbulent boundary layer of a dilute gas-particle flow past a flat plate, *Experimental Thermal and Fluid Science*, **30**, 473-483
34. WANG B., ZHANG H.Q., WANG X.L., 2006, Large eddy simulation of particle response to turbulence along its trajectory in a backward-facing step turbulent flow, *International Journal of Heat and Mass Transfer*, **49**, 415-420
35. WYDRYCH J., 2002, *Aerodynamiczne uwarunkowania procesu erozji instalacji pyłowych kotłów energetycznych*, Rozprawa doktorska, Opole
36. WYDRYCH J., SZMOLKE N., 2006, Numerical simulation of fluidization between the tubes, *Archives of thermodynamics*, **27**, 4, 245-253

37. ZHENG Y., WAN X., QIAN Z., WEI F., JIN Y., 2001, Numerical simulation of the gas-particle turbulent flow in riser reactor based on $k-\varepsilon-kp-\varepsilon p-\Theta$ two-fluid model, *Chemical Engineering Science*, **56**, 6813-6822

Obliczeniowa i eksperymentalna analiza przepływu gaz-cząstki stałe w instalacjach kotłów energetycznych w odniesieniu do zjawiska erozji

Streszczenie

W pracy przedstawiono metodę pozwalającą na ocenę prędkości zużycia erozyjnego instalacji jako funkcji jej budowy oraz warunków eksploatacji. Idea metody polega na opisie ruchu fazy gazowej równaniami Reynoldsa, uzupełnionymi modelem turbulencji. Ruch cząstek opisano metodą Lagrange'a. Następnie szacowano lokalny ubytek materiału ścianki w wyniku erozji z zastosowaniem modelu Bittera. Porównanie szczegółowych obliczeń numerycznych z wynikami pomiarów wykonano dla fragmentu instalacji pyłowej kotła BP-1150. Stwierdzono, że przy zmianie kierunku przepływu formuje się tzw. „sznur” cząstek, powodujący intensywne zużycie niektórych sekcji instalacji. Wystąpienie sekcji szczególnie narażonych na zużycie erozyjne jest uwarunkowane aerodynamiką przepływu. Stwierdzono zgodność w prognozowaniu zarówno obszarów przyśpieszonej erozji, jak i intensywności zużycia.

Manuscript received April 2, 2007; accepted for print June 4, 2007